ELSEVIER

Polymer 42 (2001) 8715–8725

polymer

www.elsevier.com/locate/polymer

Mechanical properties of blends of maleated ethylene–propylene rubber and nylon 6

O. Okada[1], H. Keskkula, D.R. Paul*

Department of Chemical Engineering, Texas Materials Institute, The University of Texas at Austin, CPE 3.454, Austin, TX 78712-1062, USA

Received 7 August 2000; received in revised form 14 May 2001; accepted 17 May 2001

Abstract

Blends of nylon 6 with maleated ethylene–propylene rubber (EPR-*g*-MA) were prepared by melt blending over the whole composition range. The reaction of the polyamide amine end groups with the grafted maleic anhydride has the potential to form thermoplastic elastomers (TPE) with controlled morphology and chemical bonding between the phases. This study focuses on the effects of nylon 6 content and crystallinity of the maleated rubber on morphological, thermal and mechanical properties of these blends. Maleated EPR with some ethylene crystallinity (H-EPR-*g*-MA) results in blends, which have better mechanical properties than those based on amorphous EPR-*g*-MA. Strain-hardening and cold-drawing were observed for both blend systems in the intermediate and polyamide-rich composition range. These effects are found to be enhanced by ethylene crystallinity in the blends. Modulus values from stress–strain measurements and dynamic, mechanical, thermal measurements are compared to predictions using a model by Hill for composite materials. Blends based on rubber with high ethylene crystallinity give better agreement with the model than those based on amorphous rubber. Phase inversion compositions derived from TEM observation, modulus measurements are compared to those calculated from the model of Avgeropoulos.

Keywords: Maleated EPR; Nylon 6; Blends

1. Introduction

Thermoplastic elastomer (TPE) compositions prepared by mixing elastomers with thermoplastics are of significant commercial interest [1–8]. Two polymeric phases, where one is rubbery and the other is either glassy or crystalline, are an essential feature of all TPEs [9]. Morphology is a key factor affecting the mechanical properties of TPE blends as in the case of block copolymers [10]. Typical commercial triblock copolymers showing TPE behavior have polystyrene spheres, about 10 nm in diameter, dispersed in a matrix of polybutadiene [11]. On the other hand, certain block copolymers (polyurethanes, polyesters, etc.) depend on a crystalline phase to act as thermally labile crosslinks. The crystalline regions appear to be continuous and highly interconnected. A morphology consisting of substantially continuous and interpenetrating crystalline and amorphous domains has been proposed [12].

Physical blending of two existing polymers may result in dual-phase continuity and phase inversion in the intermediate composition range [7,8,13–18]. An early example of a commercial product with dual-phase continuity was reported for blends of polypropylene and ethylene–propylene rubber (EPR) by Kresge et al. [7]. These authors reported that crystallinity in the ethylene–propylene copolymer phase arising from long ethylene sequences can have profound effects on the mechanical behavior of the elastomer and its blends. Baldwin and Ver Strate [19] reviewed the relationship between copolymer composition and crystallinity.

An attractive approach is to use chemical reactivity of the component polymers to achieve TPE materials of controlled morphology with chemical bonding between the phases. Blends of polyamides with maleated elastomers serve as a model for this approach. Blends of nylon 6 and EPR-*g*-MA having a continuous elastomer phase were described previously [20]. This paper focuses on the complete composition range, including the region where interpenetrating networks may be formed, for blends of nylon 6 and EPR-*g*-MA. The effects of compositions and crystallinity of EPR-*g*-MA on the morphological, thermal and mechanical properties were investigated.

* Corresponding author. Tel.: +1-512-471-5392; fax: +1-512-471-0542.
E-mail address: drp@che.utexas.edu (D.R. Paul).
[1] Present address: Bridgestone Corporation, 1 Kashio-cho, Totsuka-ku, Yokohama 244-8510, Japan.

0032-3861/01/$ - see front matter
PII: S0032-3861(01)00366-4

Table 1
Materials used in this work

Polymer	Commercial designation	Characterization[a]	Molecular weight[a]	Brabender torque[b] (N m)	Source
Nylon 6	Capron 8207F	End-group content: $[NH_2] = 47.9$ μequiv. g^{-1}, $[COOH] = 43.0$ μequiv. g^{-1}	$\bar{M}_n = 22{,}000$	5.4	Allied Signal
H-EPR-*g*-MA	Exxelor 1801	43 wt% ethylene, 53 wt% propylene, 1.21 wt% MA, crystalline[c], $T_m = 47°C$[c]	Not available	13.5	Exxon Chemical
EPR-*g*-MA	Exxelor 1803	43 wt% ethylene, 53 wt% propylene, 1.14 wt% MA, slightly crystalline[c], $T_m = 127°C$[c]	Not available	8.2	Exxon Chemical

[a] Ref. [27].
[b] Torque value taken after 10 min at 240°C and 60 rpm.
[c] Information from supplier.

2. Experimental

Table 1 describes the materials used in this work. Two commercially available ethylene/propylene copolymers grafted with maleic anhydride were obtained from Exxon Chemical, Exxelor 1803 and 1801; the former is nearly free of crystallinity and is designated here as EPR-*g*-MA while the latter has a higher level of ethylene crystallinity and is designated here as H-EPR-*g*-MA. These rubbers were blended with a nylon 6 from AlliedSignal, Capron 8207F, with a medium molecular weight ($\bar{M}_n = 22{,}000$) and balanced acid and amine end groups. An antioxidant, Irganox 1076, was added to all blends at the level of 0.2 wt% of the rubber phase. The materials were dried in a vacuum oven for a minimum of 16 h at 60°C for EPR-*g*-MA and H-EPR-*g*-MA and at 80°C for nylon 6 before melt blending.

Rheological properties were measured in a Brabender Plasticorder with a 50 cm^3 mixing head and standard rotors operated at 240°C and 60 rpm: torque values were recorded continuously during mixing of blends.

Blends were extruded twice at 240°C and 40 rpm using a Killion single screw extruder ($L/D = 30$, $D = 2.54$ cm) outfitted with an intensive mixing head after vigorously mixing all components together. The blends were injection molded into tensile bars (ASTM D638 Type I) using an Arburg Allrounder injection-molding machine. The molded specimens were stored in a vacuum desiccator in order to prevent water sorption. Those with defects and air bubbles were discarded.

Shore A hardness was examined with a Pacific Transducer durometer according to ASTM D2240. Stress–strain properties were determined by an Instron according to ASTM D412 (1980) at room temperature: the cross-head speed was varied from 5.08 to 50.8 cm/min. The permanent set after break was measured at 10 min after rupture of tensile specimens. The Young's modulus was obtained from the initial slope of the stress–strain curve at a cross-head speed of 5.08 cm/min. Standard deviation for tensile measurements was typically less than 10%.

A Polymer Laboratories DMTA was used to measure dynamic mechanical properties in cantilever mode at a medium frequency of 30 Hz from −100 to 100°C at a heating rate of 3°C/min. Heats of fusion for the blends were measured by a differential scanning calorimeter (Perkin–Elmer DSC-7) for specimens taken from injection-molded bars with a scan rate of 20°C/min. The heat of fusion of the nylon 6 or rubber phase was defined as the area under the endothermic peak for first heating. The integration of the nylon 6 melting peak was typically run from 190 to 225°C; the temperature limits for ethylene melting were 105 to 135°C for EPR-*g*-MA blends and 30 to 80°C for H-EPR-*g*-MA blends. The baseline was subtracted for each measurement.

A JEOL 200 CX transmission electron microscope (TEM) was used for morphology observation at an accelerating voltage of 120 kV using ultra-thin sections cryogenically microtomed at −50°C perpendicular and parallel to the flow direction of injection-molded bars. The nylon 6 phase was stained by a 2% aqueous solution of phosphotungstic acid for 30 min at room temperature. Average particle sizes were determined using a semi-automatic digital image analysis technique by IMAGE® software from the National Institutes of Health.

3. Morphology

The morphology of blends of both EPR-*g*-MA and H-EPR-*g*-MA with nylon 6 was evaluated over the entire composition range by transmission electron microscopy. In general, the morphology showed similar trends for both blend systems, see Fig. 1. Discrete particles of the minor phase in a matrix of the major phase were observed at 20 and 80% nylon 6; particle sizes are summarized in Table 2. A tendency for co-continuity was observed for the intermediate compositions as seen in the TEM photomicrographs for blends containing 40–60% nylon 6 in Fig. 1. An elongated nylon 6 phase was observed at 40% nylon 6; at 50% nylon 6, this was more obvious. For injection-molded bars of the blend containing 50% nylon 6, the rubber phase appears elongated in both perpendicular and parallel directions to the flow. At 60% nylon 6, phase inversion is

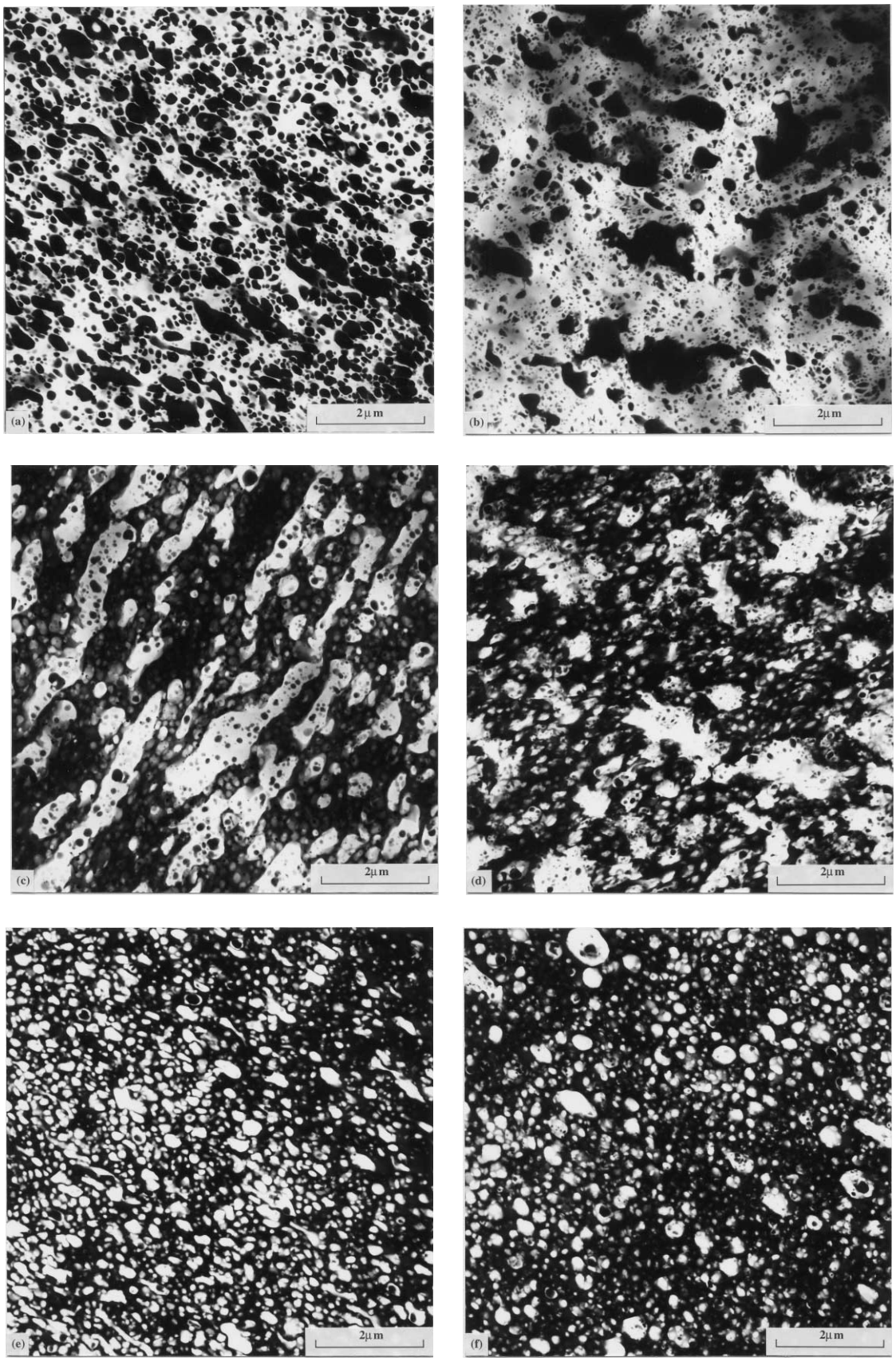

Fig. 1. TEM photomicrographs of blends of $(100 - x)\%$ maleated EPR and $x\%$ nylon 6: (a) and (b) $x = 40$, (c) and (d) $x = 50$, (e) and (f) $x = 60$; photomicrographs (a), (c) and (e) are for blends with EPR-*g*-MA; photomicrographs (b), (d) and (f) are for blends with H-EPR-*g*-MA. All views were taken in the direction perpendicular to the flow for these injection-molded compositions.

Table 2
Physical properties and morphology of nylon 6/maleated EPR blends

Rubber	% Nylon 6	Young's modulus[a] (MPa)	Yield stress[a] (MPa)	Tensile strength[a] (MPa)	Elongation at break[a] (%)	Dispersed phase	$\bar{d}_w$ (μm)	$\bar{d}_w/\bar{d}_n$
EPR-*g*-MA	0	1.62	0.21	0.15	380	–	–	–
	20	3.65	0.70	0.55	180	Nylon 6	0.23	1.43
	40	83.4	4.90	7.10	50	Nylon 6	0.30	1.50
	50	361	15.7	22.7	190	–	–	–
	60	1120	24.4	31.5	240	EPR-*g*-MA	0.22	1.39
	80	2000	41.8	34.7	140	EPR-*g*-MA	0.24	1.47
	100	2600	76.3	46.4	30	–	–	–
H-EPR-*g*-MA	0	1.36	2.39	4.80	540	–	–	–
	20	31.0	5.70	5.70	130	Nylon 6	0.12	1.52
	40	117	9.00	13.6	60	Nylon 6	0.31	3.71
	50	407	18.9	31.3	230	–	–	–
	60	629	27.4	34.9	230	H-EPR-*g*-MA	0.25	1.47
	80	1280	40.2	35.8	210	H-EPR-*g*-MA	0.19	2.00
	100	2600	76.3	46.4	30	–	–	–

[a] Extension rate = 5.08 cm/min.

complete and the rubber exists as a dispersed phase within the nylon 6 matrix. The TEM observations show that the phase inversion composition is about 50% nylon 6 for both rubber systems.

However, there are some morphological differences between EPR-*g*-MA and H-EPR-*g*-MA in these blends. First, the nylon 6 particles are smaller when the rubber matrix is H-EPR-*g*-MA than EPR-*g*-MA at 20% nylon 6. This is consistent with the higher melt viscosity [16] of H-EPR-*g*-MA than EPR-*g*-MA. Second, the EPR-*g*-MA phase shows a more elongated structure than H-EPR-*g*-MA for blends of intermediate composition: at 50% rubber, smooth elongated rubber platelets of 0.1–1 μm in thickness and 6 μm in length for EPR-*g*-MA were observed (Fig. 1c); however, rubber phases with pointed shapes of 0.3–1 μm in width and 3 μm in length were found for H-EPR-*g*-MA (Fig. 1d). The comparable rubber phase size that ranges from 0.1 to 4 μm in width was observed in continuous phase structure for ethylene–propylene rubber/polypropylene (70/30) blends by Kresge [7].

For blends in the inversion region, small particles were observed in the elongated phase indicative of a bimodal particle size distribution as noted in a paper by Kudva et al. [21]. This type of composite droplet morphology where the dispersed phase contains droplets of the matrix phase was observed for polypropylene/polycarbonate blends by Favis et al. [18].

Grafting of nylon 6 onto the maleated rubber during melt processing increases melt viscosity, which can be monitored by the torque response during melt mixing in a Brabender [20]. While nylon 6 and EPR-*g*-MA have relatively similar melt viscosities at 240°C, their blends have much higher torques as illustrated by the data in Fig. 2; indeed, the 40/60 blend of EPR-*g*-MA/nylon 6 develops a torque of more than twice that of the individual blend components. It is clear that the grafting of nylon 6 onto maleated rubber is very rapid, since the high torque of the blend is observed early in the mixing process [20]. The torque value for neat H-EPR-*g*-MA is higher than that for pure EPR-*g*-MA as seen in Table 1.

The graft copolymer formed by reaction of the nylon 6 amine end groups with maleic anhydride on EPR-*g*-MA is a compatibilizer that leads to a very fine dispersion between the nylon 6 phase and the rubber phase largely by limiting the frequency of particle–particle coalescence. In addition, the rubber/polyamide graft copolymers provide adhesion at the domain interfaces. Thus, blends of nylon 6 and maleated rubber should have a stable morphology and good adhesion between the hard and soft phases.

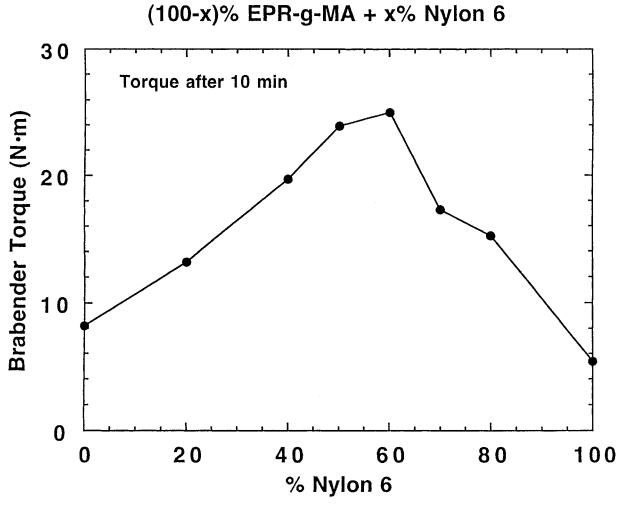

Fig. 2. Brabender torque after 10 min at 240°C and 60 rpm as a function of nylon 6 content for blends of (100 − *x*)% EPR-*g*-MA and *x*% nylon 6.

4. Mechanical properties

Shore A hardness values for the blends with a rubbery continuous phase, i.e. 0–40% nylon 6, are summarized in Table 3. The H-EPR-*g*-MA blends are harder than the EPR-*g*-MA blends; the former have values from 80 to 98, while the latter have values from 48 to 83 over this composition range. This is consistent with the higher crystallinity of H-EPR-*g*-MA.

Fig. 3 shows stress–strain diagrams for neat EPR-*g*-MA and H-EPR-*g*-MA. The latter exhibits strain-hardening while the former does not. The tensile strength of H-EPR-*g*-MA is 30 times that of EPR-*g*-MA and the elongation at break of the former is 1.4 times larger than the latter. Strain-hardening generally results from molecular alignment in the direction of the strain or from strain-induced crystallization [22]. Crystallization during stretching has been observed by X-ray diffraction for an ethylene–propylene–diene terpolymer (EPDM) lightly crosslinked with peroxide [23].

Fig. 3 also shows stress–strain diagrams for blends containing 20% nylon 6. The blend based on H-EPR-*g*-MA has a slightly lower elongation at break but much higher tensile strength than the blend based on EPR-*g*-MA. The blends do not show strain-hardening since they break just beyond the yield point. There is some evidence that the addition of the nylon 6 phase tends to inhibit crystallinity induced by deformation.

The non-recoverable deformation after failure, or set after break, during tensile testing at a cross-head speed of 5.08 cm/min shows similar trends for both blends; the amount of set decreases to quite low values when the nylon 6 content increases as seen in Table 3. The set values for blends based on H-EPR-*g*-MA are higher than those based on EPR-*g*-MA; this suggests that the crystalline phase of H-EPR-*g*-MA may undergo a typical drawing mechanism.

Fig. 4 shows stress–strain curves for blends containing 40–100% nylon 6. Strain-hardening is apparent for both blends systems when the sample contains 40% or more nylon 6. Cold-drawing was observed and elongation at break was unexpectedly high for these intermediate blends. The blends based on H-EPR-*g*-MA showed a greater degree of strain-hardening than those based on EPR-*g*-MA.

Table 3
Physical properties in the rubbery region of nylon 6/maleated EPR blends

Rubber	% Nylon 6	Hardness (Shore A)	Set after break[a] (%)	T_g (°C)
EPR-*g*-MA	0	48	48.8	−38.5
	20	55	18.1	−35.1
	40	83	3.0	−34.3
H-EPR-*g*-MA	0	80	126.5	−23.0
	20	82	32.5	−19.1
	40	98	20.7	−18.1

[a] Extension rate = 5.08 cm/min.

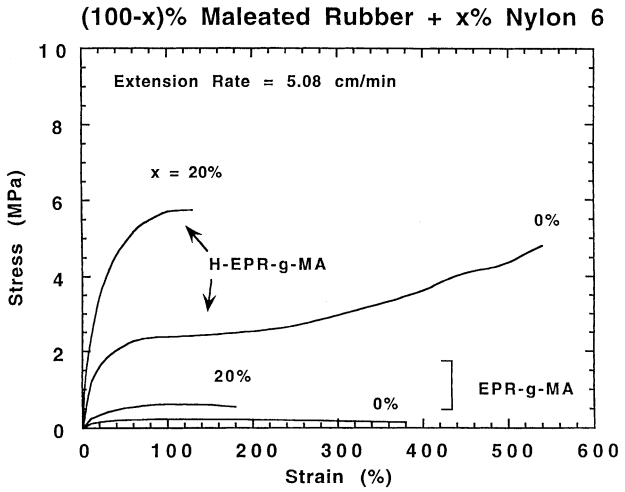

Fig. 3. Stress–strain curves for blends of $(100 - x)$% maleated EPR and x% nylon 6: $x = 0$ and 20%.

Fig. 5a provides a detailed comparison of blends based on the two maleated rubbers at 50% nylon 6. The blend based on H-EPR-*g*-MA shows higher stresses beyond the yield and a higher elongation at break. The slope in

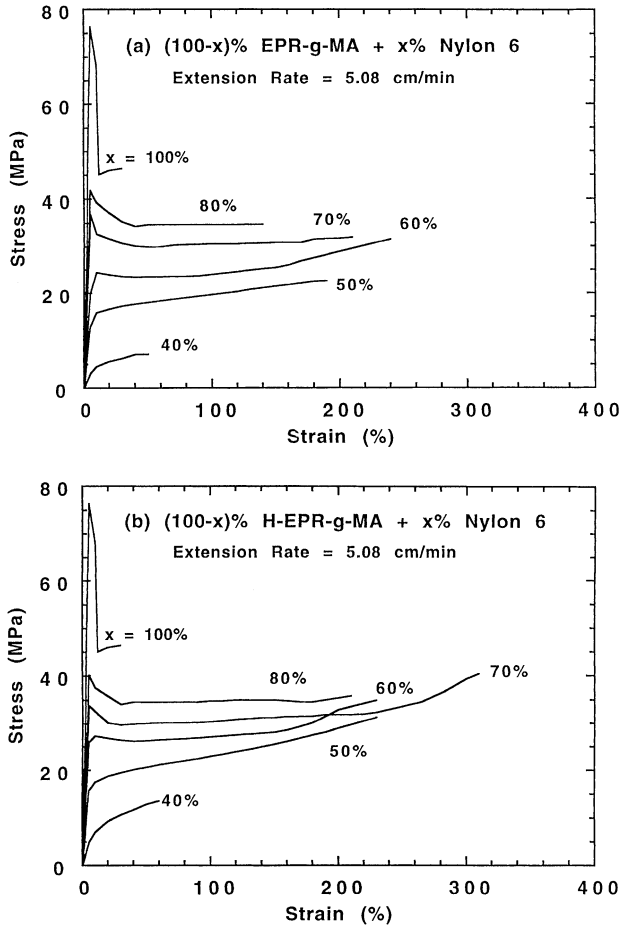

Fig. 4. Stress–strain curves for blends of $(100 - x)$% maleated EPR and x% nylon 6: $x = 40$–100%; (a) blends based on EPR-*g*-MA; (b) blends based on H-EPR-*g*-MA.

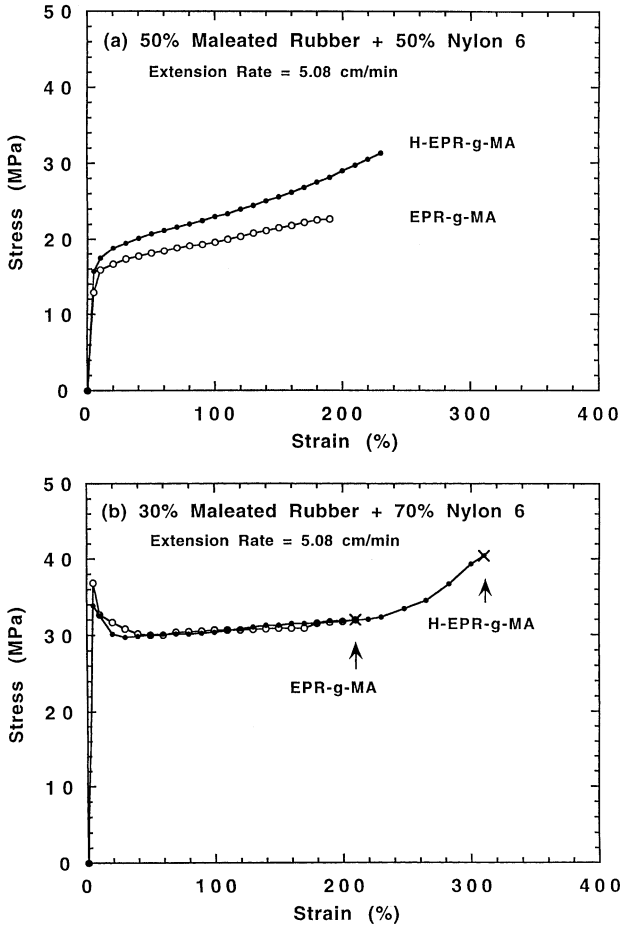

Fig. 5. Stress–strain curves for blends of $(100 - x)\%$ maleated EPR and $x\%$ nylon 6: (a) $x = 50\%$; (b) $x = 70\%$.

the post-yield region, i.e. degree of strain-hardening, is also higher for the H-EPR-*g*-MA blend. At 70% nylon 6, these differences disappear, i.e. the two stress–strain diagrams are virtually identical as seen in Fig. 5b. Both blends show the same yielding and cold-drawing behavior until 200% elongation. However, the ultimate properties, tensile strength and elongation at break, are greater for the blends based on H-EPR-*g*-MA.

The effect of crosshead speed on the stress–strain curve was examined. For blends containing less than 40% nylon 6, stress levels at a given strain were higher for faster test speeds [20]; however, for blends containing 50% nylon 6 or more, the effect of test speed on the stress–strain diagram was substantially less as illustrated in Fig. 6.

Blends containing 60% or more of nylon 6 showed a distinct yield point, while blends containing less than 50% nylon 6 did not. In the latter case, the reported yield stress was defined as the stress where the tangents of the initial and final parts of the load–elongation curve intersect [24]. Fig. 7 shows the effect of nylon 6 content on the yield stress. The blends based on H-EPR-*g*-MA show higher yield stress than those based on EPR-*g*-MA when the nylon 6 content is less than 60% as mentioned earlier (Fig. 5a). This may be

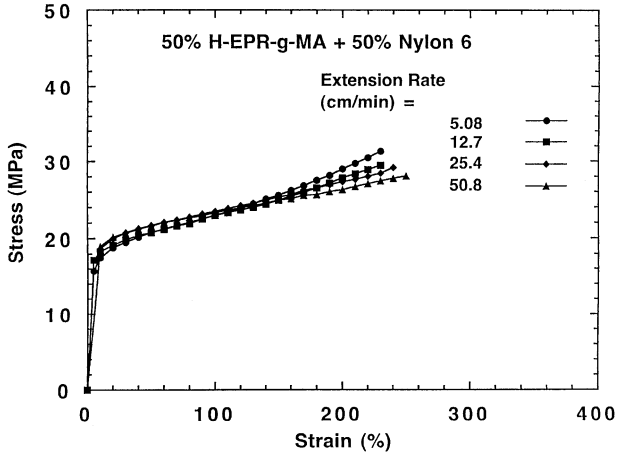

Fig. 6. Stress–strain curves for blends of 50% maleated EPR and 50% nylon 6 at various extension rates.

explained on the basis of the higher crystallinity of H-EPR-*g*-MA. However, for the blends containing more than 70% nylon 6, there is no distinguishable difference in the yield stress.

Fig. 8 compares the ultimate properties of these blends to that expected from simple additivity (dotted line). The ultimate tensile strength and elongation at break show similar trends for the blends based on either rubber. When the rubber is the continuous phase, both strength and elongation are below the additive values, which suggest that the nylon 6 particles in the rubber matrix do not cause effective reinforcement [20]. When nylon 6 forms the continuous phase, the tensile strength is equal to or higher than the additive value and the elongation at break is always higher than average. The H-EPR-*g*-MA based blends generally have superior ultimate properties.

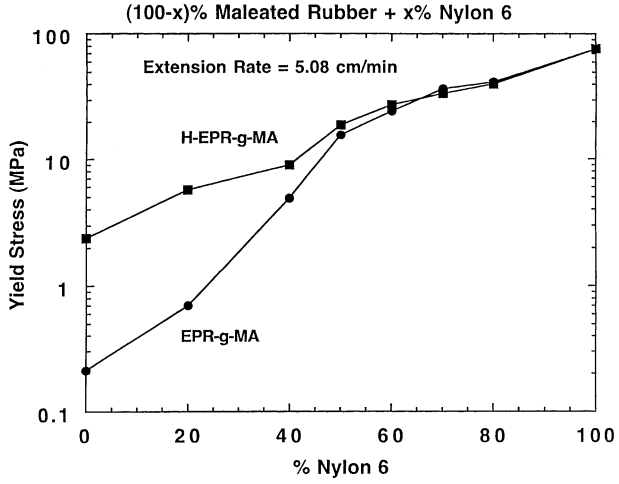

Fig. 7. Yield stress as a function of nylon 6 content for blends of $(100 - x)\%$ maleated EPR and $x\%$ nylon 6.

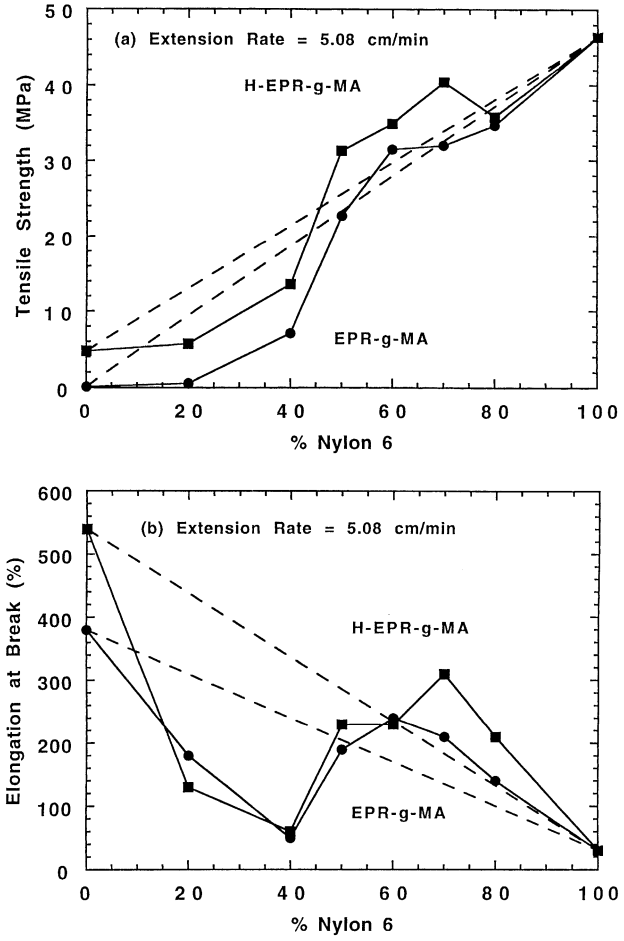

Fig. 8. Ultimate properties as a function of nylon 6 content for blends of $(100 - x)$% maleated EPR and x% nylon 6: (a) tensile strength; (b) elongation at break.

5. Thermal and dynamic mechanical analysis

Fig. 9 shows DSC thermograms for blends containing 40% nylon 6 prepared from the two different maleated elastomers. Both materials show a peak at about 217°C from melting of nylon 6. However, they show distinctly different peaks at a lower temperature due to melting the crystallinity formed from sequences of ethylene units in the rubber, namely, a peak at 125°C for EPR-*g*-MA blends and a peak at 45°C for H-EPR-*g*-MA blends. The heat of fusion for the latter peak is larger than that of the former. Ver Strate et al. [25] have reported that major melting point depression results from addition of the comonomer in ethylene–propylene copolymers and showed two different melting points at about 120 and 50°C, which are in the range observed in this study. The melting peaks for nylon 6 and the rubber do not depend significantly on blend composition; these phases are not expected to exhibit co-crystallization like that reported for blends of EPDM and low-density polyethylene (LDPE) [26].

Fig. 10a shows how the heat of melting of the ethylene sequences varies with the nylon 6 content of the blends. The

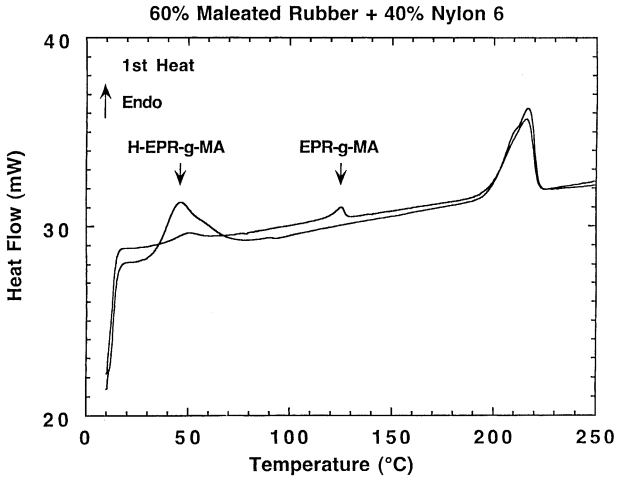

Fig. 9. DSC thermograms of first heat cycle for blends of 60% maleated EPR and 40% nylon 6.

blends based on H-EPR-*g*-MA show a much higher heat of fusion than those based on EPR-*g*-MA, especially for lower content of nylon 6. The larger values of the ultimate tensile properties for the H-EPR-*g*-MA blends can be explained by

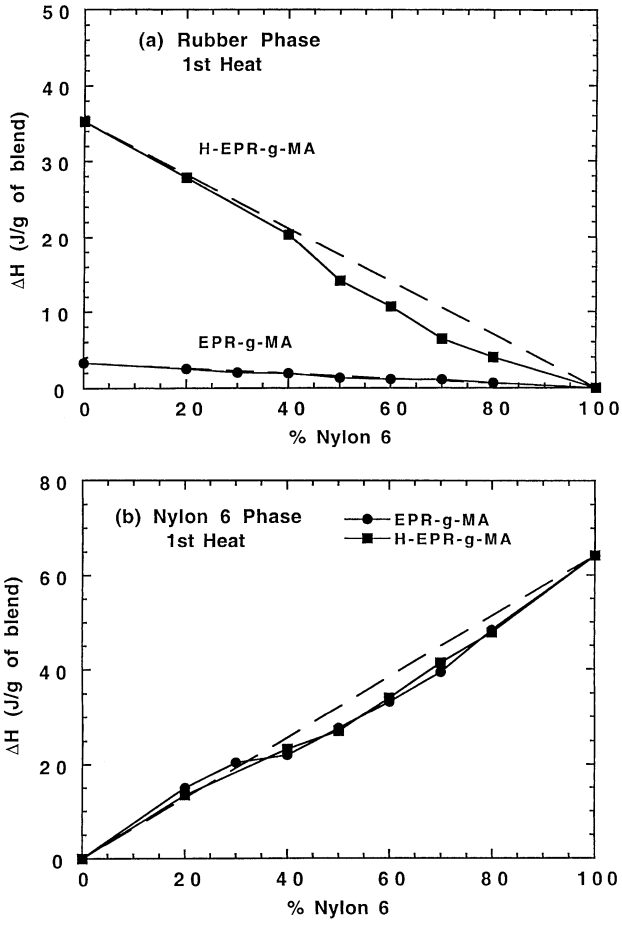

Fig. 10. Heat of fusion for melting peaks of (a) rubber phase and (b) nylon 6 phase from a first heat as a function of nylon 6 content.

Table 4
Glass transition temperature and tan δ at peak from DMTA for nylon 6/maleated EPR blends

Rubber	% Nylon 6	Rubber phase		Nylon 6 phase	
		T_g (°C)	tan δ at peak maximum	T_g (°C)	tan δ at peak maximum
EPR-*g*-MA	0	−38.5	1.10	N/A	N/A
	20	−35.1	0.97	N/A	N/A
	40	−34.3	0.57	52.3 (shoulder)	N/A
	50	−38.2	0.17	59.3	0.16
	60	−45.1	0.089	59.5	0.14
	70	−45.6	0.064	60.0	0.14
	100	N/A	N/A	65.8	0.18
H-EPR-*g*-MA	0	−23.0	0.21	N/A	N/A
	20	−19.1	0.18	N/A	N/A
	40	−18.1	0.13	61.6 (shoulder)	N/A
	50	−30.0	0.068	64.6	0.15
	60	−31.4	0.046	64.8	0.12
	70	−32.8	0.038	64.0	0.12
	80	−36.3	0.031	60.5	0.11
	100	N/A	N/A	65.8	0.18

these larger heats of fusion, i.e. larger crystallinity of ethylene in the blends. For the rubbery blends, in which the nylon 6 particles are dispersed in the rubber matrix phase, higher crystallinity provides more extensive tie points that act as crosslinks in the deformation field. On the other hand, for the intermediate and nonrubbery blends, larger crystallinity results in larger strain-hardening as mentioned earlier.

Fig. 10b shows the relation between the heat of fusion of nylon 6 and the content of nylon 6 in the blend. For blends containing less than 40% nylon 6, the experimental values are very close to what is expected by additivity. However, for blends containing from 50 to 80% nylon 6, the observed heats of fusion are lower than additive. Oshinski [27] reported that reactive blends have lower crystallinity than expected from additivity. Grafting of nylon 6 onto rubber reduces the crystallization rate of nylon 6 because the melt viscosity increases as seen in Fig. 2 [28].

Fig. 11 shows the dynamic mechanical storage modulus (E') and loss tangent (tan δ) for the blends based on H-EPR-*g*-MA as a function of temperature; similar data have been reported previously for blends based on EPR-*g*-MA [20]. The locations of the observed tan δ peaks associated with the glass transitions of the rubber and nylon 6 are given in Table 4. Both blends showed similar trends including a small increase in the T_g of about 5°C for the rubber phase as the nylon 6 content increases from 0 to 40%. As the nylon 6 content is increased further from 50 to 70 or 80%, the T_g of the dispersed rubber decreases below that of the neat rubbers. This behavior is also observed for grafted polybutadiene rubbers in ABS materials [29] and is attributed to dilatational stresses stemming from differences in the volume contraction of the phases on cooling. A tan δ peak associated with the β-relaxation of nylon 6 occurs at −26.5°C near the glass transition for these two rubbers.

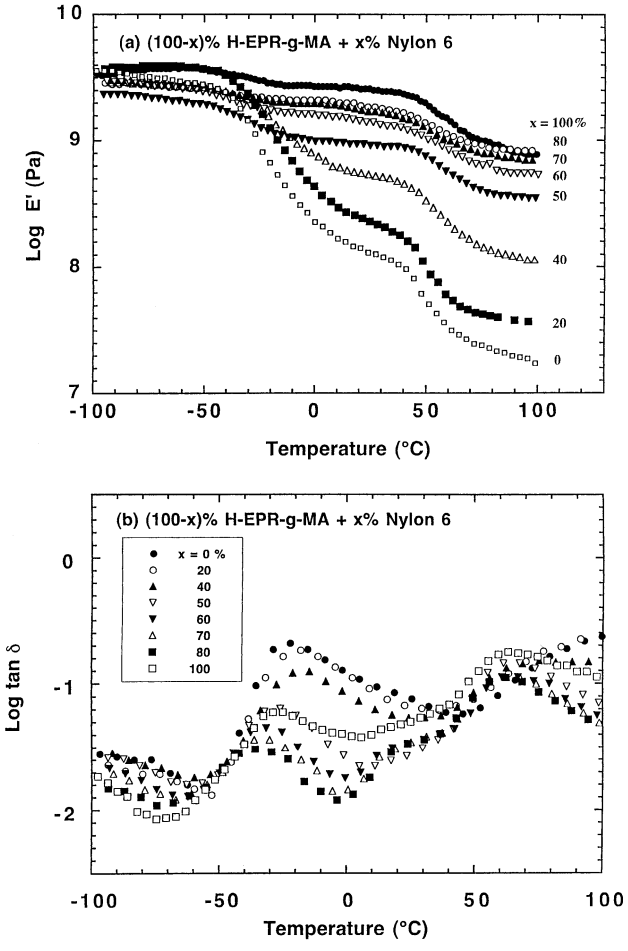

Fig. 11. Viscoelastic data as a function of temperature for blends of (100 − *x*)% H-EPR-*g*-MA and *x*% nylon 6: dynamic storage modulus (a) and tan δ (b). Similar data for blends with EPR-*g*-MA have been reported previously [20].

The values of T_g for the rubber phase of H-EPR-*g*-MA blends are higher than those of EPR-*g*-MA blends, because of the higher crystallinity of H-EPR-*g*-MA. However, it should be noted that there is little difference in the elongation at break of those blends as mentioned above.

The storage modulus E' of each blend shows a significant decrease at the glass transition of the rubber and the nylon 6 phase and at the melting point of nylon 6 (off the scale used in the current graphs). It is interesting to note that a significant decrease in modulus occurs at about 50°C for blends based on H-EPR-*g*-MA that contain less than 50% of nylon 6. This results from melting of the crystalline phase of H-EPR-*g*-MA as seen by DSC; however, no corresponding tan δ peak was observed.

The size of the tan δ peak associated with the rubber phase is shown as a function of nylon 6 content in Fig. 12. When the nylon 6 phase is dispersed in a matrix of rubber, the EPR-*g*-MA blends have higher values of tan δ than the H-EPR-*g*-MA blends. This behavior is consistent with a lower level of crystallinity as found by DSC.

Experimental values of the modulus from stress–strain testing at 5.08 cm/min, E, are shown for blends of nylon 6 with EPR-*g*-MA and with H-EPR-*g*-MA over the entire composition range in Fig. 13. The observed values are compared to theoretical predictions (solid lines) calculated using a self-consistent theory proposed by Hill [30]. This model is expressed in the form

$$\left[\frac{\phi_1 K_1}{K_1 + (4/3)G} + \frac{\phi_2 K_2}{K_2 + (4/3)G}\right] + 5\left[\frac{\phi_1 G_2}{G - G_2} + \frac{\phi_2 G_1}{G - G_1}\right] + 2 = 0 \quad (1)$$

where K is the bulk modulus and G the shear modulus of the blend, the subscript indicates the corresponding component i, and ϕ_i the volume fraction of component i.

The tensile, E_i, bulk, K_i, and shear, G_i, moduli of each component (or blend) are interrelated via Poisson's ratio, ν_i, by the following:

$$K_i = \frac{E_i}{3(1 - 2\nu_i)} \quad \text{and} \quad G_i = \frac{E_i}{2(1 + \nu_i)} \quad (2)$$

Poisson's ratio was assumed to be 0.49 for EPR-*g*-MA and 0.33 for nylon 6 [31] and to be a linear function of composition for the blends.

Fig. 14 shows similar comparison between calculated and experimental values of the dynamic storage modulus. The calculated values are from the Hill equation assuming that Young's modulus, E, can be replaced with the complex modulus [32], E^*, and that in turn E^* is approximately equal to the storage modulus [33], E'. There is little difference between E and E' for blends, in which nylon 6 phase is continuous, while E' is larger than E for blends where nylon 6 is a discrete phase in a rubber matrix. Both E and E' are higher for the blends based on H-EPR-*g*-MA than those based on EPR-*g*-MA, because of the larger crystallinity of

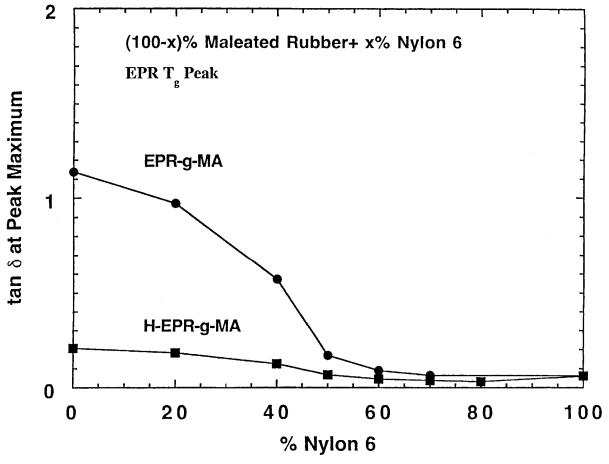

Fig. 12. tan δ at peak maximum for rubber phase T_g as a function of nylon 6 content for blends of $(100 - x)$% maleated EPR and x% nylon 6.

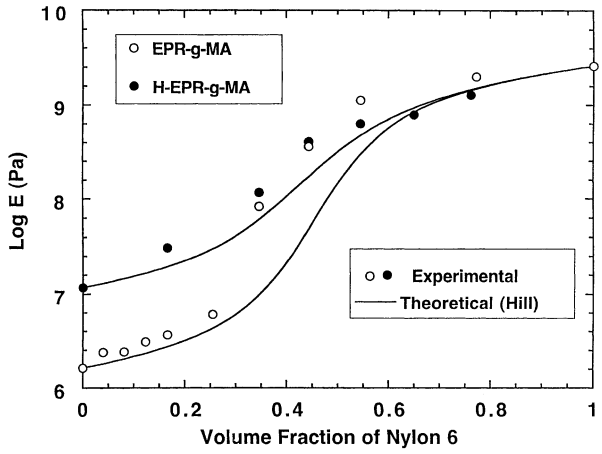

Fig. 13. Effect of nylon 6 content on Young's modulus, E, from stress–strain diagrams for blends of nylon 6 and maleated EPR: (○) EPR-*g*-MA and (●) H-EPR-*g*-MA.

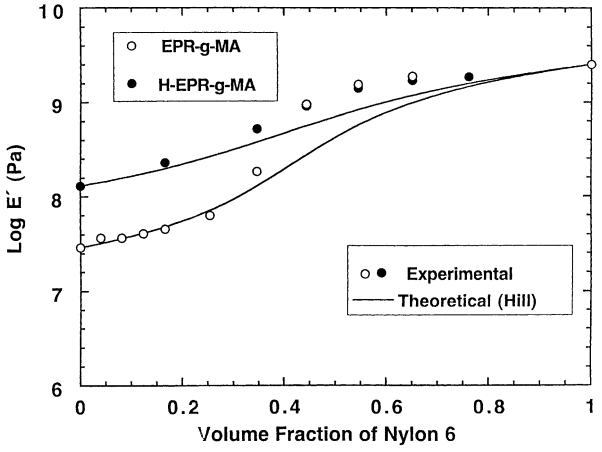

Fig. 14. Effect of nylon 6 content on dynamic storage modulus, E', from dynamic mechanical testing for blends of nylon 6 and maleated EPR: (○) EPR-*g*-MA and (●) H-EPR-*g*-MA.

the former. When compared at constant values of modulus (either E or E'), especially in the phase inversion region, the volume fraction of nylon 6 from the experimental result is lower than that from the theoretical curve as seen in Figs. 13 and 14. This deviation between apparent and actual volume fractions is larger for EPR-*g*-MA blends than for H-EPR-*g*-MA blends. This may be caused by an anisotropic structure, i.e. more elongated morphology for EPR-*g*-MA blends than for H-EPR-*g*-MA as seen by TEM.

6. Phase inversion behavior

Dual phase continuity, i.e. phase inversion, occurs when the slope of log E or log E' as a function of composition is steepest [13]. The phase inversion compositions from curves calculated by the Hill equation are 44 vol.% (50 wt%) for both E and E' for both rubber systems. However, the inversion points from the experimental modulus values occur at lower nylon 6 content as seen in Table 5.

There are several models to predict phase inversion composition for polymer blends [16]. Recently, Mekhilef [14] suggested that the Avgeropoulos model, in which torque ratio is equated with the volume fraction ratio, predicts the point of phase inversion better than various semi-empirical models using the viscosity ratio. In the Avgeropoulos model, the inversion point composition is expressed as [15]

$$\frac{T_1}{T_2} = \frac{\phi_1}{\phi_2} \tag{3}$$

where T_i is the torque of polymer i. The inversion point predicted by the Avgeropoulos model for EPR-*g*-MA blends is 40 vol.% (46 wt%) and that for H-EPR-*g*-MA is 29 vol.% (34 wt%). Experimental values from TEM observations and modulus curves are compared to the predicted values in Table 5. The predicted value for the EPR-*g*-MA blends was found to be close to the values from TEM. In the case of H-EPR-*g*-MA blends, the predicted value was less than the experimental values. Favis [16] pointed out that morphology of polymer blends is affected by various material parameters such as viscosity ratio, composition, elasticity, shear stress and interfacial modification. Recently, Bourry [17] showed that both elastic and viscous effects should be considered for blends of high-density polyethylene and polystyrene. These factors other than composition no doubt account for some of the discrepancy between the predicted values and the experimental values observed in this study.

Table 5
Phase inversion volume fraction of nylon 6 for nylon 6/maleated EPR blends

Rubber phase	Calculated[a]	TEM	Young's modulus	Storage modulus
EPR-*g*-MA	0.40	ca. 0.44	0.32	0.40
H-EPR-*g*-MA	0.29	ca. 0.44	0.40	0.40

[a] Calculated by torque ratio (Eq. (3)).

7. Conclusions

The morphology, thermal properties and mechanical behavior for blends of nylon 6 with EPR-*g*-MA and H-EPR-*g*-MA have been examined over the whole composition range. Generally, both types of rubber show similar morphological features; however, the following differences were noted. First, the rubbery blends of H-EPR-*g*-MA yield smaller nylon 6 particles than that of EPR-*g*-MA at low contents of nylon 6. Second, in the inversion range, the EPR-*g*-MA phase is rather smooth and elongated, while the H-EPR-*g*-MA phase is pointed and discrete. The size and shape of the dispersed rubber particles are similar for the two types of rubber when nylon 6 is the continuous phase.

Two typical tensile behaviors were observed for both blend systems based on EPR-*g*-MA and H-EPR-*g*-MA, viz., homogeneous deformation without a well-defined yield point and inhomogeneous deformation with necking and cold-drawing. These behaviors depend on morphology of the blends. The former is observed for the rubbery blends where nylon 6 spheres are dispersed in a rubber matrix and for the intermediate blends. The latter is observed for the polyamide-rich blends where rubber particles are dispersed in a nylon 6 matrix phase.

H-EPR-*g*-MA blends have superior mechanical properties compared to EPR-*g*-MA blends. Strain-hardening, which may be caused by strain-induced crystallization of ethylene sequences, is observed for neat H-EPR-*g*-MA. However, adding nylon 6 results in poor ultimate properties in the rubbery region, where tensile strength and elongation at break are lower than expected from additivity. Hardness, tensile strength, set after break, static Young's modulus and dynamic storage modulus for H-EPR-*g*-MA blends indicate larger values than those for EPR-*g*-MA blends. These results are consistent with higher crystallinity of H-EPR-*g*-MA than EPR-*g*-MA. For the intermediate blends (40 to 60% nylon 6), strain-hardening is observed for both blend systems. Yield stress and tensile strength at break for the H-EPR-*g*-MA blends are higher than those based on EPR-*g*-MA. The former blends have steeper slopes in the post yield region than the latter blends. Both elongation at break and tensile strength increase as nylon 6 content is increased in the intermediate composition range. On the other hand, tensile strength increases but elongation at break decreases with nylon 6 content in the composition range, where the rubber phase is dispersed. Stress–strain curves show cold-drawing behavior and are virtually identical for both blend systems in this composition region. However, elongation at

break for EPR-*g*-MA blends is lower than that for H-EPR-*g*-MA blends at 70 and 80% nylon 6. The former blends break before the stress can increase, while the latter blends do not.

Thermal analysis shows that the H-EPR-*g*-MA blends have higher crystallinity based on ethylene sequences than the EPR-*g*-MA blends, although the latter has the higher melting temperature. The rubber phase values of tan δ at peak maximum are higher for EPR-*g*-MA blends than for H-EPR-*g*-MA blends, which is consistent with the difference in crystallinity between two rubbers. Experimental modulus values were compared to those predicted by the Hill theory. The difference between these values is small when the nylon 6 content is at either extreme for both blends. However, in the intermediate region (i.e. 20–80% nylon 6), H-EPR-*g*-MA blends show better agreement with the model than do EPR-*g*-MA blends.

The phase inversion compositions from TEM and modulus curves were compared to predicted values from the model of Avgeropoulos. The predicted value for the EPR-*g*-MA blends is close to that found by TEM but differs from that indicated by the experimental modulus curve. In the case of H-EPR-*g*-MA blends, the predicted value is less than the experimental value.

Acknowledgements

This research was supported by Bridgestone Corp. The authors express their appreciation to AlliedSignal Inc. and Exxon Chemical Co. for supplying various materials used in this research.

References

[1] Wolfe Jr JR. In: Legge NR, Holden G, Schroeder HE, editors. Thermoplastic elastomers: a comprehensive review. New York: Hanser, 1987. p. 117–31.
[2] Bohn L. Rubber Chem Technol 1968;41:495.
[3] Reed MC, Harding J. Ind Engng Chem 1949;41:675.
[4] Hammer CF. In: Paul DR, Newman S, editors. Polymer blends, vol. 2. New York: Academic Press, 1978. p. 219–41.
[5] Hartman PF, Eddy CL, Koo GP. Rubber world 1970;163(1):59.
[6] Ramos-Devalle LF, Ramirez RR. Rubber Chem Technol 1982;55:1328.
[7] Kresge EN. In: Paul DR, Newman S, editors. Polymer blends, vol. 2. New York: Academic Press, 1978. p. 293–318.
[8] Ranalli R. In: Whelan A, Lee KS, editors. Developments in rubber technology, Thermoplastic rubbers, vol. 3. Barking: Applied Science, 1982. p. 21–57.
[9] Legge NR, Davison S, De La Mare HE, Holden G, Martin MK. Appl Polym Sci. Tess RW, Poehlein GW, editors. ACS Symp Ser 1985;285:175–217 (2nd ed.).
[10] Molau GE. In: Aggarwal SL, editor. Block polymers. New York: Plenum Press, 1970. p. 79.
[11] Beecher JF, Marker L, Bradford RD. J Polym Sci, Part C 1969;26:117.
[12] Cella RJ. J Polym Sci, Symp Ed 1973;42:727.
[13] Jordhamo GM, Manson JA, Sperling LH. Polym Engng Sci 1986;26:517.
[14] Mekhilef N, Verhoogt H. Polymer 1996;37:4069.
[15] Avgeropoulos GN, Weissert FC, Biddison PH, Böhm GGA. Rubber Chem Technol 1976;49:93.
[16] Favis BD. In: Paul DR, Bucknall CB, editors. Polymer blends, vol. 1. New York: Wiley, 2000. p. 501–37.
[17] Bourry D, Favis BD. J Polym Sci, Polym Phys 1998;36:1889.
[18] Favis BD, Chalifoux JP. Polymer 1988;29:1761.
[19] Baldwin FP, Ver Strate G. Rubber Chem Technol 1972;45:709.
[20] Okada O, Keskkula H, Paul DR. Polymer 1999;40:2699.
[21] Kudva RA, Keskkula H, Paul DR. Polymer 1998;39:2447.
[22] Nielsen LE, Landel RF. Mechanical properties of polymers and composites. 2nd ed. New York: Marcel Dekker, 1994 (p. 299).
[23] Bassi IW, Corradini P, Fagherazzi G, Valvassori A. Eur Polym J 1970;6:709.
[24] Ward IM, Hadley DW. An introduction to the mechanical properties of solid polymers. Chichester: Wiley, 1993 (p. 221).
[25] Ver Strate G, Wilchinsky ZW. J Polym Sci, Part A-2 1971;9:127.
[26] Starkweather Jr HW. J Appl Polym Sci 1980;25:139.
[27] Oshinski AJ, Keskkula H, Paul DR. Polymer 1996;37:4891.
[28] Martuscelli E, Riva F, Sellitti C, Silvestre C. Polymer 1985;26:270.
[29] Morbitzer L, Kranz D, Humme G, Ott KH. J Appl Polym Sci 1976;20:2691.
[30] Hill R. J Mech Phys Solids 1965;13:213.
[31] Brandrup J, Immergut EH, editors. 3rd ed. Polymer handbook, vol. V/113. New York: Wiley, 1989.
[32] Uemura S, Takayanagi M. J Appl Polym Sci 1966;10:113.
[33] Ward IM, Hadley DW. An introduction to the mechanical properties of solid polymers. Chichester: Wiley, 1993 (p. 63).